

Article

Not peer-reviewed version

---

# XPS and ARXPS for Characterizing Multilayers of Silanes on Gold Surfaces

---

Giulio Casula , [Marzia Fantauzzi](#) , [Bernhard Elsener](#) , [Antonella Rossi](#) \*

Posted Date: 21 February 2024

doi: 10.20944/preprints202402.1193.v1

Keywords: Surface Chemistry; Surface Analysis,; XPS; ARXPS; Freshly cleaved gold; MPTMS, APTES, Thickness calculation



Preprints.org is a free multidiscipline platform providing preprint service that is dedicated to making early versions of research outputs permanently available and citable. Preprints posted at Preprints.org appear in Web of Science, Crossref, Google Scholar, Scilit, Europe PMC.

Copyright: This is an open access article distributed under the Creative Commons Attribution License which permits unrestricted use, distribution, and reproduction in any medium, provided the original work is properly cited.

Article

# XPS and ARXPS for Characterizing Multilayers of Silanes on Gold Surfaces

G. Casula, M. Fantauzzi, B. Elsener and A. Rossi \*

Dipartimento di Scienze Chimiche e Geologiche, Università degli Studi di Cagliari, 09042 Cagliari, Italy.

\* Correspondence: rossi@unica.it

**Abstract:** XPS and ARXPS characterization of surface layers resulting from the functionalization of polymers such as PVC modified with MPTMS and APTES is challenging due to the signals overlap, deriving both from the substrate and the functionalized layers. In this work, a freshly cleaved, ideally flat gold surface was used as carbon-free model substrate functionalized with MPTMS and subsequently grafted with APTES. Avoiding the overlap of signals from carbon atoms present in the substrate, the signals in the C1s, O1s, Si2p, S2p and N1s high-resolution spectra could be assigned to the MPTMS / APTES functionalized layer only and the curve fitting parameters could be determined. Quantitative analysis was in very good agreement with the expected stoichiometry of the functionalized layer, confirming the adopted curve fitting procedure. In addition, it was found that one molecule of APTES grafted two MPTMS via silane groups. ARXPS allowed determining the thickness of the functionalized layers: MPTMS thickness was found to be 0.5 (0.2) nm, MPTMS + APTES thickness 1.0 (0.2) nm in good agreement with Avogadro model calculations. This approach can be considered a powerful tool for characterising functionalized surfaces of more complex systems by XPS.

**Keywords:** freshly cleaved gold; surface chemistry; XPS and ARXPS; thickness calculation; MPTMS and APTES

---

## 1. Introduction

By modifying the surface of the material, it is possible to achieve tailor-made properties different from those in the bulk, thereby opening new perspectives for scientific and technological applications. One way to achieve surface functionalization is the formation of self-assembled monolayers (SAMs) that can be defined as the arrangement of molecules adsorbed onto a solid surface that can aggregate spontaneously from solution or gas phase [1] and [2]. SAMs are versatile systems that have been applied in the surface modification of a variety of materials such as metals and polymers. Due to this versatility SAMs can be exploited for different application ranging from UV-lithography [3] to the production of antimicrobial polymers [4]. Historically gold has been used as substrate for growing thin layer such as SAMs on its surface with organic thiols. In fact, organosulfur compounds such as thiols, disulfides and sulfides can react with a gold substrate by spontaneous adsorption either from liquid or from the vapor phase forming SAMs [5]. Among the organosulfur compounds, 3(mercaptopropyl)-trimethoxysilane (MPTMS) is widely used in the surface modification of gold surfaces due to the presence of thiol groups that can strongly bind to the gold surface [6,7]. The formation of SAMs by immersion of the substrate into a dilute ethanolic solution of thiols is time dependent and require 12-18 hours of immersion for obtaining a well-organized SAMs [5]. Reduced immersion time may lead to the formation of a weak interaction between sulphur atoms of the thiols onto the gold surface, such as dithiolate [8–10]. Moreover, thiols in ambient conditions and in presence of water may react forming disulfides that can physisorbed onto the sulphur substrate [11]. Another molecule that was used to functionalize silicon-based substrates is aminopropyltriethoxysilane (APTES) due to the presence of the Si-OEt group. An example of APTES monolayer on gold has been reported by Yang et alii [12]; in that work the surface of a gold electrode was firstly modified with potassium hydroxide (KOH) in order to have a hydroxyl activated gold surface thus allowing the subsequent anchoring of APTES monolayer through the

reaction of -OH groups at the surface of gold with Si-OEt groups. No characterization of the surface by XPS was reported. MPTMS and APTES can also be used together to form a multi-layered system through the reaction of the Si-O groups that are present in both the molecules. The reaction between MPTMS and APTES has been proposed for the functionalization of polymers [4,13] as intermediate stage for the surface functionalization of medical-grade PVC to confer antimicrobial property, but no examples of this functionalization are reported in the literature for gold that can be considered an excellent model system for validating the characterization approach based on surface analytical techniques.

X-ray photoelectron spectroscopy (XPS) is a powerful analytical tool that is exploited for the characterization of thin layers since it is a surface sensitive method and allows obtaining in-depth compositional information on layers with a thickness ranging from 0.5 nm and 10 nm [14] depending on the kinetic energy of the photoemitted electrons and the photoelectron inelastic mean free path ( $\lambda$ , IMFP) in [15,16], and on the material and on the emission angle. Angle-resolved XPS (ARXPS) can be successfully used for the characterization of thin layers such as SAMs [17] since it is possible the determination of the in-depth distribution and of the thickness of monolayers applying various approaches [18,19]. Many examples of gold surfaces functionalization with thiols are reported in the literature [1,20,21] for different applications; some examples of gold surfaces functionalized with MPTMS are reported even if XPS was not exploited in this investigation [22]. On the other hand, XPS results on MPTMS reacted with a glass surface were reported by Penna et alii [23]. Graf et alii [24] applied XPS to APTES monolayers onto a silicon surface and proposed few possible arrangements of this molecule based on the XPS results. While the literature abounds with examples of surface modification involving MPTMS or APTES investigated by XPS, no papers report the use of XPS and ARXPS for a comprehensive characterization of the overlayer made of MPTMS on gold and further grafted with APTES.

In this paper the overlayer formed by MPTMS on gold, subsequently grafted with APTES, are investigated by XPS and ARXPS to get an insight into the spatial arrangement, thickness, and composition of the functionalization layer on gold surfaces. Furthermore, XPS and ARXPS characterization of this model system allows the determination of the curve-fitting parameters for the C 1s signal but also for the other functional groups of the functionalization layer.

This is crucial for the development of an analytical strategy and an important reference for whom might be involved in the XPS characterization of more complex system such as polymers functionalized with the same protocol, allowing the identification and the clear distinction of the components of C 1s signal that belong to the functionalization layer from those of the polymer substrate. Additionally, the spatial distribution of the different functional groups and the thickness of the overlayer will be investigated by ARXPS [18,25]. This information might allow ascertaining the possible three-dimensional arrangements of the functionalization layer and the investigation of the formation of a three-dimensional cross linking of the silanes as proposed in [26] on the basis of FTIR investigation. Finally, another aim of the present investigation is to provide evidence of the formation of a single layer of APTES after its grafting to MPTMS.

## 2. Experimental

### 2.1. Materials

(3-mercaptopropyl) trimethoxysilane (MPTMS) and 96% ethanol were purchased from VWR (Italy) and used without further purification; aminopropyltriethoxysilane (APTES) was purchased from Sigma-Aldrich (Germany). Both MPTMS and APTES are soluble in ethanol and insoluble in water. The chemical formulae of MPTMS and APTES are given in Figure 1.

Gold samples were provided by C. Passiu depositing 80 nm-thick gold films on silicon wafers through electron-beam evaporation following the procedure described in [27]. Template stripping was performed immediately before functionalisation to minimize the presence of adsorbed carbon and oxygen species due to the contact with the atmosphere. The roughness ( $R_a$ ) of the gold samples was measured by atomic force microscopy (AFM) and resulted to be equal to 0.3 (0.1) nm [28].

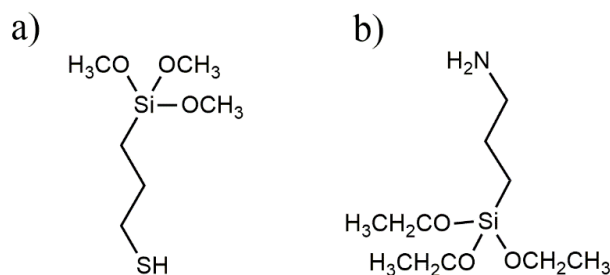


**Figure 1.** (3-mercaptopropyl) trimethoxysilane (MPTMS) (a) and aminopropyltriethoxysilane (APTES) (b) molecular formulae.

### 2.2. MPTMS Functionalization

Fresh-cleaved gold samples were initially immersed in ethanol for one hour and then dipped into a 10% solution of MPTMS in ethanol for one hour to allow the reaction with MPTMS. This experimental condition is analogous to the one adopted for forming a MPTMS overlayer onto a food-grade PVC surface [24] and allows limiting the multilayer formation.

The samples were then immersed again in ethanol for one hour after the functionalization. No visible change of the surface was observed. The gold samples functionalized with MPTMS are named M-Gold in the following and the reaction scheme is shown in Figure 2.

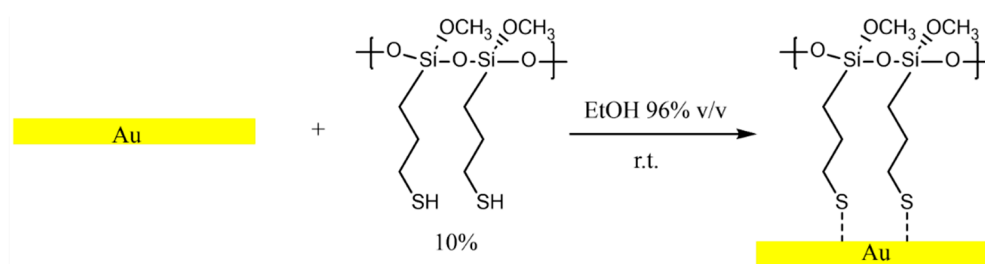


**Figure 2.** Reaction scheme of fresh-cleaved gold surface with MPTMS forming a monolayer on gold (M-gold) performed at room temperature. The dashed bond indicate that the sulphur may be weakly bonded to the gold surface.

### 2.3. APTES Functionalization

The M-gold samples were immersed in a solution of 7.5 mM of APTES in a mixture of ethanol 96% v/v and ammonia 20% v/v for 1h (70% ethanol 20% of ammonia). The outward-facing Si-O groups in MPTMS on the M-gold surface react with the Si-O groups present in APTES, allowing the grafting of APTES onto the M-Gold surface. The reaction scheme between M-Gold and APTES is reported in Figure 3. The final product was named A-gold. Following the functionalization, A-gold samples were immersed in ethanol for 1 h to remove the non-grafted APTES. The samples were dried with an argon flux and were immediately transferred to the x-ray spectrophotometer.

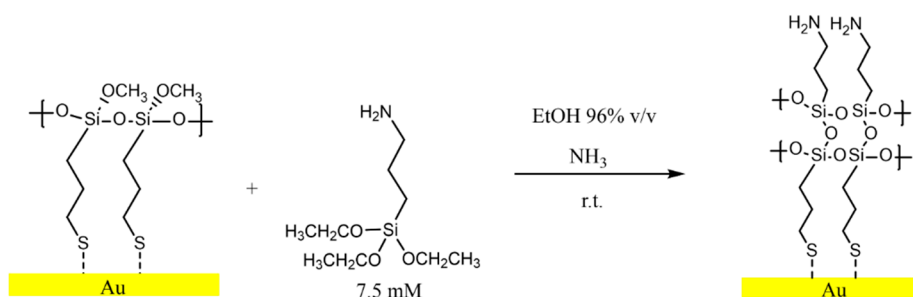


**Figure 3.** Reaction scheme of M-Gold exposed to APTES 7.5 mM solution. The dashed bond indicate that the sulphur may be weakly bonded to the gold surface.

#### 2.4. X-ray Photoelectron Spectroscopy (XPS) and Angle-Resolved X-ray Photoelectron Spectroscopy (AR-XPS)

The XPS measurements were carried out with a Theta Probe spectrometer (Thermo Fisher Scientific, East Grinstead, UK). The base pressure in the analysis chamber was  $1 \times 10^{-9}$  mbar or below, the pressure remained unchanged during the experiments thus suggesting a good stability of the samples under vacuum. Only one sample was introduced in the analysing chamber at a time to avoid sample cross contamination. No charge neutralization was required during the acquisition of the spectra. The spectra were collected using a monochromatic Al-K $\alpha_{1,2}$  source ( $h\nu = 1486.6$  eV) selecting a nominal 400  $\mu\text{m}$  spot size with a power of 100 W. All spectra were acquired in the fixed analyser transmission (FAT) mode and the pass energy (PE) was set at 200 eV for the survey spectra and at 150 eV for the high-resolution ones and a step size of 0.1 eV.

Acquisition time for the survey spectra was 10 minutes and for the high-resolution spectra was in total equal to 30 minutes. These conditions allowed obtaining a good signal-to-noise ratio in a minimum time to limit sample damage induced by the X-ray beam.

A periodic calibration following ISO 15472:2010 was performed to verify the linearity of the binding energy scale. The Au 4f $_{7/2}$  was used as internal reference at 83.97 eV, and in these conditions the FWHM at the peak height was found to be 1.2 (0.1) eV. The energy resolution measured on the Ag3d $_{5/2}$  signal at 368.20 eV was 1.27 eV in these conditions. The high-resolution spectra were resolved into their components after background subtraction using the iterative U3-Tougaard model [29].

The apparent composition in at% was calculated using the peak areas (intensities) of the high resolution spectra following the curve-fitting procedure and corrected for relative sensitivity factors that take into account the Scofield's photoionization cross section [30], the asymmetry factor [30], the intensity/energy response function [31] and the inelastic mean free path [32]; a table with the parameters is provided in the Supplementary Material (Table S1).

High-resolution ARXPS spectra were acquired in angle resolved lens mode: this mode allows the parallel collection of angle-resolved data without tilting the sample with respect to the lens axis thanks to a 2D detector. In this work the photoelectrons were detected from 16 different angles ranging from 24.9° - 81.1° to the normal. Thanks to this combination of radians lens and 2D-detector, the analysed area does not change during the analysis. Emission angle is defined as the angle formed by the direction of the photo-emitted electrons and the normal to the sample surface. In this work, only spectra acquired at angles below 60° were considered in order to mitigate the potential effects of elastic scattering that may occur at angles greater than 60° [26]. This could affect the accuracy of thickness estimation, apparent concentration, and relative depth plot calculations [33,34]. The pass energy was set at 150 eV, the energy resolution was 1.27 eV (FWHM height of Ag3d $_{5/2}$ ) the angular signature was collected at 150 eV pass energy and an example is provided in the supplementary (Figure S1). The total acquisition time was 35 minutes. The conditions here selected allowed the achievement of good reproducibility of the results. The spectra were processed either by CasaXPS software (version 2.3.24PR1.0 Casa Software Ltd, Teignmouth, UK) [35] or by Avantage (v4.88, Thermo Fisher Scientific, East Grinstead, UK) software). The spectra were obtained on three different samples. On each sample three analysis points were selected. The binding energy values, and the atomic composition are provided as mean values. The standard deviation is given in parentheses.

### 3. Results

#### 3.1. X-ray Photoelectron Spectroscopy of Freshly Cleaved Gold before Functionalization

XPS was used for characterising the freshly cleaved gold surface before and after functionalization with MPTMS (M-Gold). M-Gold grafted with APTES is named A-Gold. XPS allows the identification of the elements, of their chemical state and the determination of the surface composition. The survey spectrum of freshly cleaved gold before the functionalization is reported in Figure 4a. The spectrum shows the presence of a barely visible C 1s signal due to a short-time exposure to the ambient, together with peaks ascribed to gold; no O 1s signal was detectable.

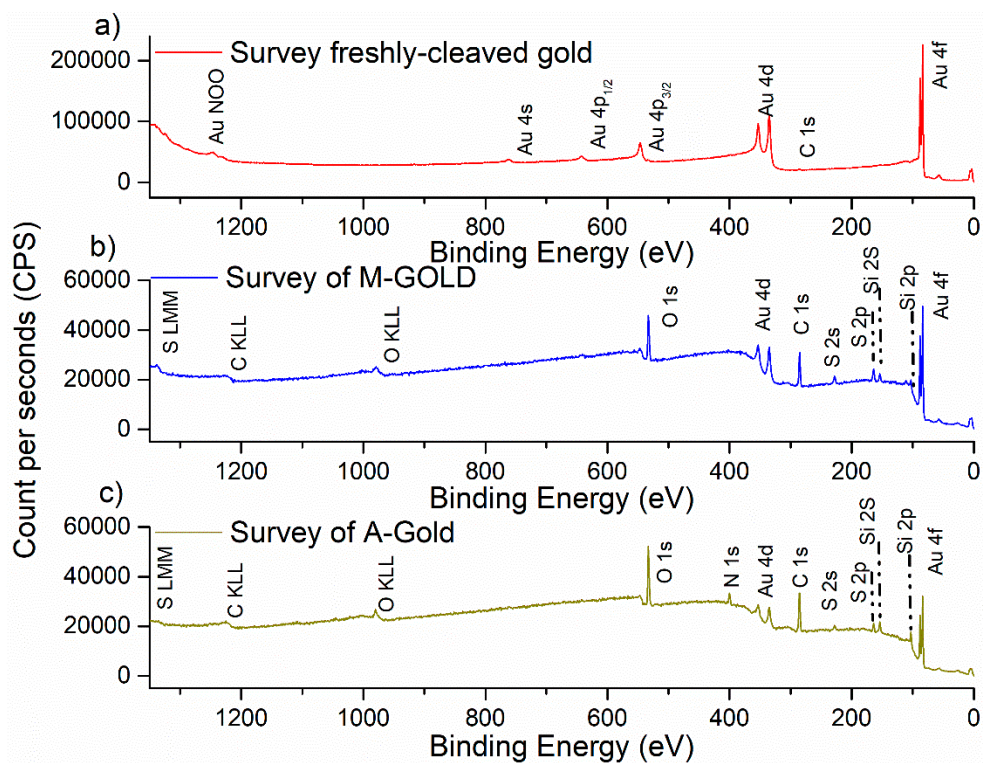


**Figure 4.** Survey spectra of (a) fresh-cleaved gold, (b) gold after functionalization with MPTMS (M-Gold), (c) M-Gold after grafting with APTES (A-gold).

Figure 5 shows the curve-fitted high-resolution Au 4f signal after background subtraction with U 3 Tougaard model. Au 4f peaks were fitted with a doublet due to the spin-orbit coupling being the energy separation between the 4f<sub>7/2</sub> and 4f<sub>5/2</sub> taken equal to 3.7 eV and the area ratio equal to 4:3. The full width at half-maximum height (FWHM) was 1.2 eV for both the components. The details on the line-shape of the signals and on the constraints adopted for the curve fitting are reported in Table 1 and are in agreement with the literature [28,36].

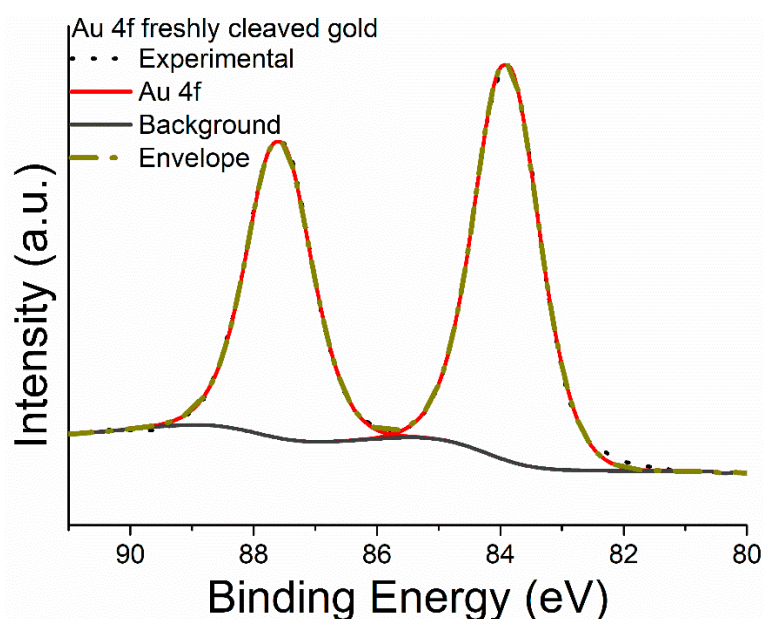


**Figure 5.** Example of high-resolution spectrum of Au 4f signal acquired on freshly cleaved gold sample.

### 3.2. X-ray Photoelectron Spectroscopy after Functionalization with MPTMS

XPS spectra were acquired after the immersion of the freshly cleaved gold samples in the 10% MPTMS solution for one hour and subsequent immersion in ethanol. The survey spectrum of the MPTMS functionalized samples (Figure 4b) showed the presence of silicon (Si 2p, Si 2s), sulphur (S 2p, S 2s), oxygen (O1s) and carbon (C 1s) signals attributed to the presence of a MPTMS surface layer. The Au 4f signals are still revealed but compared to the freshly cleaved sample (Figure 4a) their intensity is attenuated by the organic overlayer. The presence of the overlayer is also responsible for the change in the background shape after the immersion of the freshly cleaved gold in the MPTMS solution.

**Table 1.** Curve-fitting parameters used for processing the most intense signals of freshly cleaved gold, M-Gold and A-Gold.

	FWHM (eV)	Background	Line shape	Constrains
Au 4f	1.2 (0.1)		GL(50) T(5.5)	Area Au 4f <sub>5/2</sub> = Area Au 4f <sub>7/2</sub> x 0.75 FWHM Au 4f <sub>5/2</sub> = FWHM Au 4f <sub>7/2</sub> x 1
C 1s contamination	1.6 (0.1)		GL(30)	FWHM C 1s Contamination = FWHM C 1s C-Si, C-C x 1
C 1s C-Si, C-C	1.6 (0.1)		GL(30)	
C 1s C-S	1.6 (0.1)		GL(30)	FWHM C 1s C-S = FWHM C 1s C-Si, C-C x 1 Area C 1s C-S=Area C-Si, C-C x 0.5
C 1s methoxide	1.6 (0.1)		GL(30)	FWHM C 1s methoxide = FWHM C 1s C-Si, C-C x 1
C 1s of the NH(C*O)O group	1.6 (0.1)	U 3 Tougaard	GL(30)	FWHM C 1s of the NH(C*O)O group = FWHM C 1s of C-Si, and of C-C x 1
O 1s Si-O-Si	1.8 (0.1)		GL(30)	
O 1s of the NH(CO)O* carbamate group	1.8 (0.1)		GL(30)	FWHM O 1s NH(CO)O* = FWHM O 1s Si-O-Si x 1
O 1s of the NH(CO*)O carbamate group	1.8 (0.1)		GL(30)	Area O 1s NH(CO*)O = Area O 1s NH(CO)O* x 1 FWHM O 1s NH(CO)O* = FWHM O1s Si-O-Si x 1
S 2p	1.6 (0.1)		GL(30)	Area S 2p <sub>1/2</sub> = Area S 2p <sub>3/2</sub> x 0.5 FWHM S 2p <sub>1/2</sub> = FWHM S 2p <sub>3/2</sub> x 1 BE 2p <sub>1/2</sub> = BE 2p <sub>3/2</sub> + 1.16

			Area Si 2p <sub>1/2</sub> = Area Si 2p <sub>3/2</sub> x 0.5
Si 2p	1.5 (0.1)	GL(30)	FWHM Si 2p <sub>1/2</sub> = FWHM Si 2p <sub>3/2</sub> x 1 BE 2p <sub>1/2</sub> = BE 2p <sub>3/2</sub> + 0.6
N 1s -NH <sub>2</sub>	1.6 (0.1)	GL(30)	
N 1s -NH <sub>3</sub> <sup>+</sup>	1.6 (0.1)	GL(30)	FWHM N 1s -NH <sub>3</sub> <sup>+</sup> = FWHM N 1s -NH <sub>2</sub> x 1
N 1s -N*H(CO)O	1.6 (0.1)	GL(30)	FWHM -N*H(CO)O = FWHM N 1s -NH <sub>2</sub> x 1

Representative high-resolution C 1s, S 2p, Si 2p, O 1s and Au 4f spectra are shown in Figure 6. The spectra were acquired for investigating the chemical state of the elements and for the quantification. The binding energies of the different components of C 1s, O 1s, S 2p and Si 2p signals revealed on the M-gold samples are listed in Table 2 where also the apparent atomic concentration (at%) of each component of the elements present in the MPTMS layer is reported. The apparent composition was calculated assuming the in depth-homogeneity of the layer.

Au 4f signal (Figure 6a) was resolved in the spin-orbit components applying the same parameters adopted for the freshly cleaved gold sample.

The curve fitting of the C 1s signal after the reaction (Figure 6b) resulted in four components: a peak at 284.9 eV attributed to carbon in C-Si and CH<sub>2</sub> of the MPTMS, two more peaks assigned to the C-S and CH<sub>3</sub>O at 285.9 eV and 287.0 eV respectively, and a peak at 285 eV that was attributed to the aliphatic component of the contamination layer (represented by the dotted curve in Figure 6b). The area of the component ascribed to C-Si and CH<sub>2</sub> and of the C-S component was constrained to be 2:1 as expected from the stoichiometry of MPTMS (Figures 1 and 2) assuming the formation of a monolayer of MPTMS; the areas of the other components were not constrained. (Table 1).

S 2p peaks were curve-fitted with a doublet due to spin-orbit coupling (Figure 6c). The area ratio between S 2p<sub>3/2</sub> and S 2p<sub>1/2</sub> was constrained to be equal to 2:1 and the energy separation was 1.16 eV. The binding energy value of the S 2p<sub>3/2</sub> component was found to be 163.7 (0.1) eV (Table 2). The O 1s signal (Figure 6d) was fitted with a single component having the peak maximum at 532.6 eV ascribed to the -O-Si component of the MPTMS following [37].

The Si 2p high-resolution spectrum (Figure 6e) consists of a doublet due to the spin-orbit coupling with an energy separation between the 2p<sub>3/2</sub> and 2p<sub>1/2</sub> components of 0.6 eV and an area ratio equal to 2:1. (Table 1) The binding energy of Si 2p<sub>3/2</sub> component was found to be 102.3 eV (Table 2) and it is in agreement with the value reported in [38] for silicon involved in CH<sub>2</sub>-Si-O bonds in MPTMS.

The results of the quantitative analysis of the MPTMS functionalized layer (excluding the signal of gold from the substrate) are shown in Table 2. The S : Si ratio of 1 : 1 confirms the expected stoichiometry of the MPTMS layer. It is worth noting that only 4% methoxide is detected instead of 12%, this might be due to the hydrolysis of Si-OCH<sub>3</sub> bonds to yield silanols, the majority of which couple to form siloxanes forming a three-dimensional cross-linking of the Si-O-Si bond. A comparison with the expected composition of the functionalized layer is discussed in section 4.3.2.

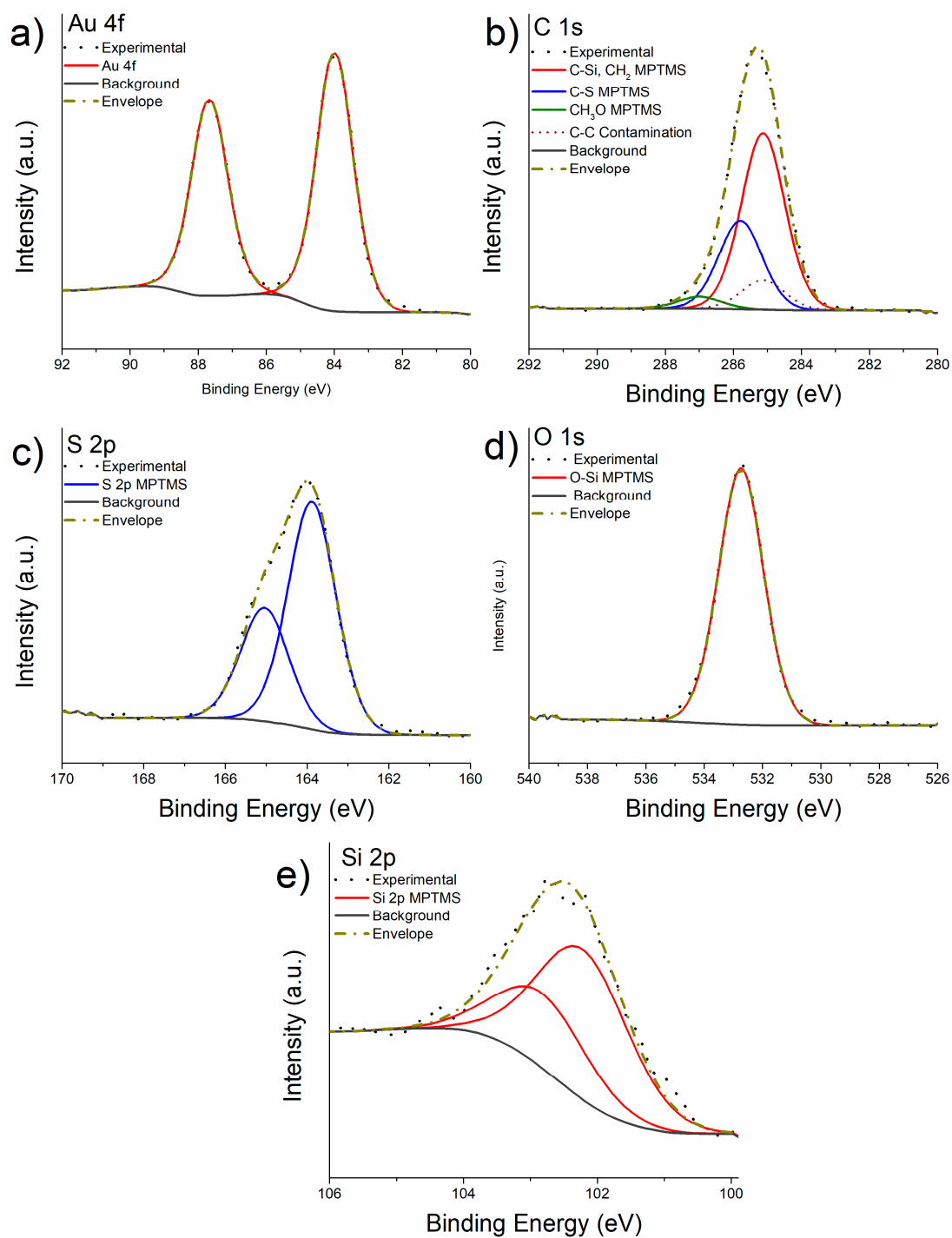


**Figure 6.** High-resolution spectra of Au 4f (a), C 1s (b), S 2p (c), O 1s (d), and Si 2p (e) signals of the fresh-cleaved gold after functionalization with MPTMS.

**Table 2.** Binding energies values (eV) and composition (at%) for M-Gold samples. Mean values over three independent measurements are reported; the standard deviations are given in parentheses.

	Binding energy (eV)	M-Gold 10% at %
C 1s C-Si, C-C	284.9 (0.1)	27 (2)
C 1s C-S	285.9 (0.2)	13 (1)

C 1s Methoxide (-OCH <sub>3</sub> )	287.0 (0.1)	4 (1)
O 1s Si-O-Si	532.6 (0.1)	29 (3)
S 2p	163.7 (0.1)	13 (2)
Si 2p	102.3 (0.2)	13 (2)

### 3.3. X-ray Photoelectron Spectroscopy of MPTMS Functionalized Gold after Grafting with APTES

The samples functionalized with MPTMS (M-Gold samples) were dipped into an APTES solution 7.5 mM in ethanol and ammonia for 1h. A representative survey spectrum following the immersion in APTES solution is shown in figure 4c; in addition to the signals of carbon, oxygen, sulphur and silicon, the nitrogen, N 1s, signal is detected supporting the presence of APTES grafted to MPTMS on the gold surface sample. Gold signals are still detected but at lower intensity than in M-gold samples (Fig. 4b).

The magnified version of Figure 4a, 4b and 4c is provided in the supplementary material file (Figures S2, S3 and S4).

The high-resolution spectra of Au 4f, C 1s, N1s, O 1s, S 2p and Si 2p are shown in Figure 7. The same curve-fitting parameters and constraints used for M-Gold spectra (Table 1) were applied in this case. The binding energy values of the different components of the most intense photoelectron lines and the results of the quantitative analysis are provided in Table 3.

No difference in the line shape of Au 4f signal was observed after the functionalization of gold with MPTMS and APTES (Figure 7a). The C 1s high-resolution spectrum (Figure 7b) was fitted with five components, four of these are ascribed to the MPTMS-APTES overlayer and one is assigned to aliphatic carbon (contamination). The red curve was attributed to the C-Si, CH<sub>2</sub> at 285.3 eV of the MPTMS-APTES chain and it was constrained to be in a 2:1 ratio with the component at 286.0 eV that is ascribed to CH<sub>2</sub>-S and CH<sub>2</sub>-NH<sub>2</sub> component as expected from the stoichiometry considering the model shown in Figure 3. The C-Si, CH<sub>2</sub> signal following the reaction with APTES was shifted by +0.4 eV compared to the same signal observed in M-Gold (Table 2) being the binding energy of the former and the latter 284.9 eV and 285.3 eV respectively. Carbon atoms bonded to sulphur and nitrogen atoms are found at 286 eV in agreement with the literature [23,24].

N 1s signal (Figure 7c) was multi-component and processed considering three components at 399.8 eV, 400.8 eV and 402.2 eV attributed to the -NH<sub>2</sub>, NHCOO carbamate, and NH<sub>3</sub><sup>+</sup>, respectively, as the presence of the three functional groups is commonly observed in similar systems [24]. The -NH<sub>2</sub> component can be attributed to the free amine groups of the APTES layer, while the NH<sub>3</sub><sup>+</sup> contribution may be due to weak hydrogen bond interaction between amine groups of two or more APTES chains. Finally, the component at 400.8 eV is attributed to NHCOO carbamate due to the reaction between the CO<sub>2</sub> and amine groups of the APTES; this is substantiated also by the presence of the COO signal at 289 eV in the C 1s spectra [24,39], according to the reaction presented in [40].

The O 1s signal shape (Figure 7d) suggests the presence of two additional small components aside the main O-Si contribution observed also in M-Gold. These two new components at 534.2 eV and 531.1 eV can be assigned to the C-O and C=O of the carbamate, their ratios were constrained to be 1:1.

S 2p and Si 2p signals (figure 7e and 7f) have been resolved applying the same curve-fitting model used for the M-Gold spectra. The Si 2p and S 2p peak showed a shift of 0.4 eV towards higher binding energy values compared to the binding energy observed for the M-Gold sample (Table 2).

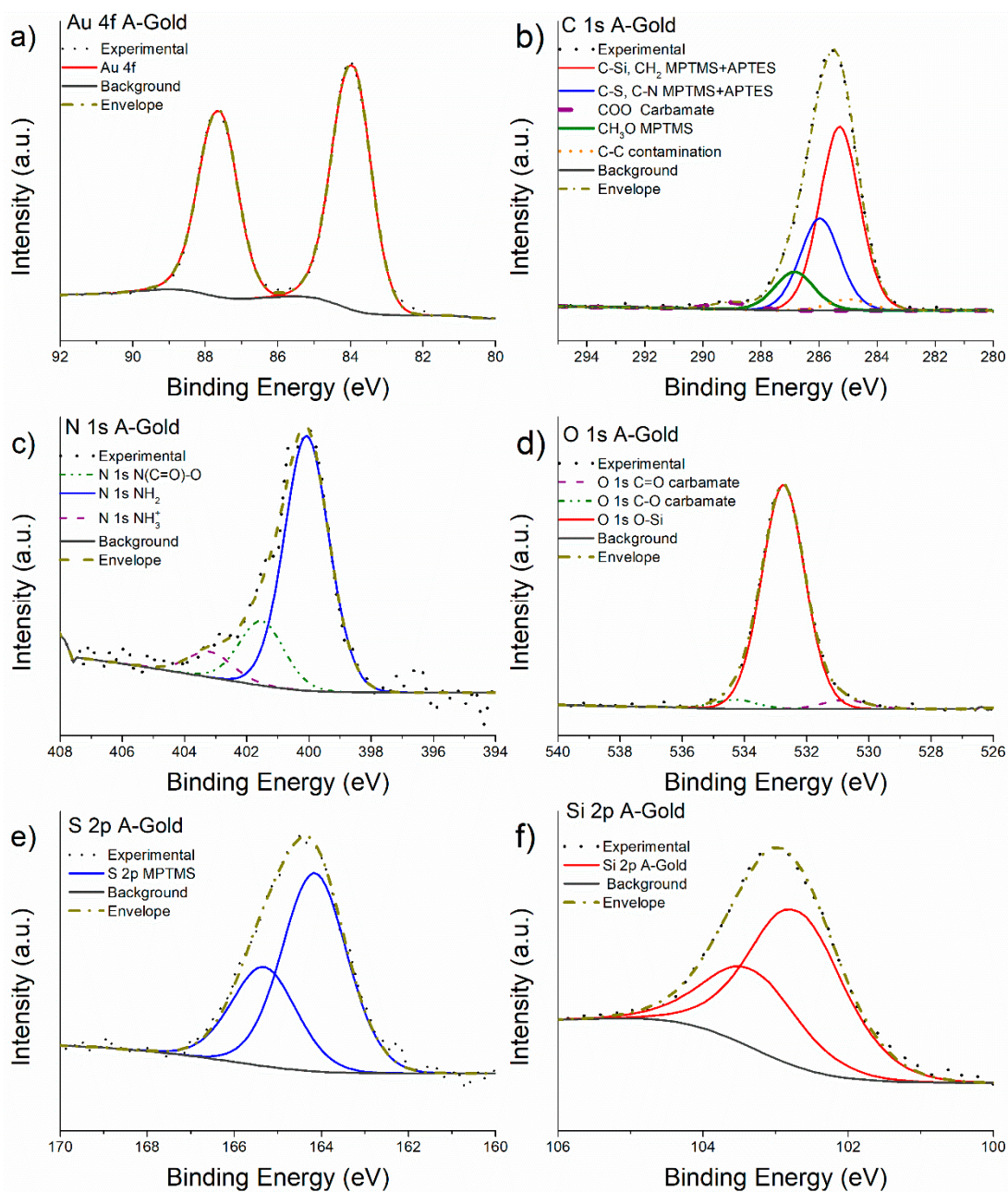


**Figure 7.** High-resolution spectra of Au 4f (a), C 1s (b), N 1s (c), O 1s (d), S 2p (e) and Si 2p (f) recorded on A-Gold sample.

**Table 3.** Binding energies and quantitative analysis results for A-Gold samples. Mean values over three independent measurements are reported; the standard deviation is given in parentheses.

	Binding energy (eV)	A-Gold at %
C 1s C-Si, C-C	285.3 (0.1)	27 (1)
C 1s C-S	286.0 (0.2)	13 (1)
C 1s Methoxide	287.0 (0.2)	4 (1)
C 1s O-C=O carbamate	289.2 (0.2)	1.2 (0.2)
O 1s C=O* carbamate	531.1 (0.2)	1.3 (0.5)
O 1s Si-O-Si	532.7 (0.1)	23 (2)

O 1s O <sup>-</sup> -C carbamate	534.2 (0.1)	1.3 (0.5)
S 2p	164.1 (0.1)	10 (2)
Si 2p	102.7 (0.1)	15 (1)
N 1s -NH <sub>2</sub>	399.8 (0.3)	3 (1)
N 1s NHCOO	400.8 (0.3)	1.2 (0.4)
N 1s -NH <sub>3</sub> <sup>+</sup>	402.2 (0.3)	0.6 (0.1)

The quantitative analysis of the XPS measurements on the A-gold surface (functionalized with MPTMS and grafted with APTES) shows that the atomic ratio between Si 2p and S 2p signals is 1.5:1 (Table 3); this might suggest that two molecules of MPTMS on the M-gold samples react with one molecule of APTES. Moreover, the total concentration of N 1s signal is about 5 at%, thus resulting in a S to N ratio equal to 2:1 supporting a reaction between MPTMS and APTES, which is not in a 1 to 1 ratio. A comparison with the expected composition of the functionalized layer is given in the discussion section (section 4.3.2).

#### 3.4. Angle-Resolved X-ray Photoelectron Spectroscopy on MPTMS Functionalized Gold M-Gold

High-resolution spectra (Figure S5) of C 1s, O 1s, Si 2p, Au 4f and S 2p were acquired on the MPTMS functionalized gold samples at different emission angles; with increasing emission angle the sampling depth decreases. The surface sensitivity is higher at high emission angles. Signals of all the elements were revealed at all emission angles, the intensity of Au 4f signals is the highest at 24.9 degree, that of Si 2p is highest at 58.6 degree. The apparent concentrations in atomic percentage (obtained from the quantitative analysis at each emission angle) plotted versus the emission angle are shown in Figure 8a for M-Gold samples. It can be noted that the apparent concentration of carbon C-Si and of O-Si are the highest and they increase with the emission angle, while the concentration of gold (Au 4f) decreases (Figure S6). The apparent concentrations of sulphur and silicon do not vary (within the standard deviation) with the emission angle.

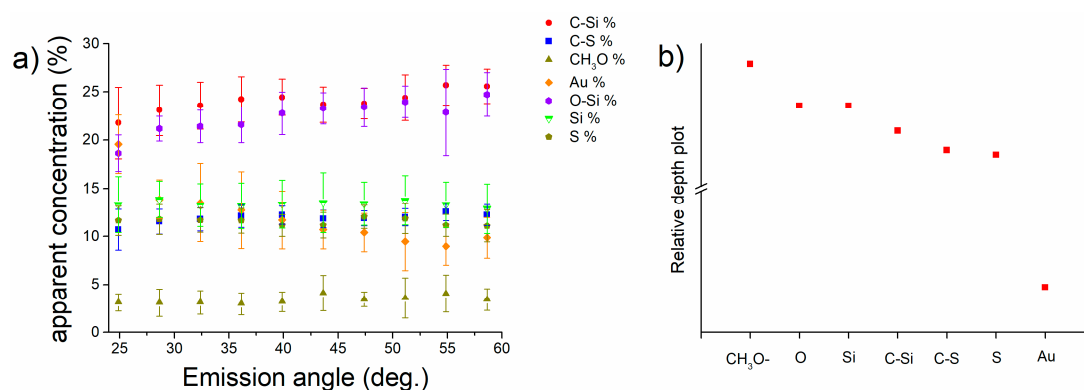


**Figure 8.** Apparent concentration (%) versus emission angle calculated for Au, Si, S, C-Si, O-Si, CH<sub>3</sub>O and C-S (a) and relative depth plot (b) for M-gold.

The relative depth plot (calculated by the Avantage software v. 5.932 by Thermo Fisher) that indicates the in-depth distribution of the different elements and functional groups (Figure 8b) is obtained by calculating the logarithm of the area ratio of the peak at near grazing angles (58.6 degrees) to that at near normal emission angle (24.8 degrees). The expected behaviour according to the scheme proposed in Figure 2 is confirmed, suggesting that the MPTMS molecules might be adsorbed on the gold surface via sulphur atoms and the Si-O functional groups are facing the outer part of the layer.

#### 3.5. Angle-Resolved X-ray Photoelectron Spectroscopy of A-Gold

The high-resolution spectra of the ARXPS experiments conducted on A-Gold samples are reported in Figure S7. The A-Gold ARXPS spectra showed the presence of N 1s signal as also revealed

in standard lens mode (section 3.3), and its presence is detected at emission angles greater than 28.6 degrees. This suggests that nitrogen is part of the outermost surface as might be expected from the scheme depicted in Figure 3. Moreover, Figure 9 shows that the apparent concentration of the S 2p signal decreases at high emission angles, indicating its presence in the inner part of the overlayer. (see section 3.4).

The apparent concentration of carbon bound to silicon, nitrogen, gold, sulphur, silicon, and oxygen bound to silicon for A-Gold at the different emission angle is shown in Figure 9a. Au 4f apparent concentration decreases at higher emission angles as observed in the case of M-Gold samples. In this case also sulphur concentration decreases at higher emission angles, while the apparent concentrations of C-Si and N increase. Oxygen and silicon apparent atomic concentrations are nearly independent on the angle. The relative depth plot for A-Gold samples based on the ARXPS results (Figure 9b) shows that nitrogen should be located at the outermost surface, while sulphur and gold are in the most internal layer as expected from the reaction scheme of A-gold (Figure 3).

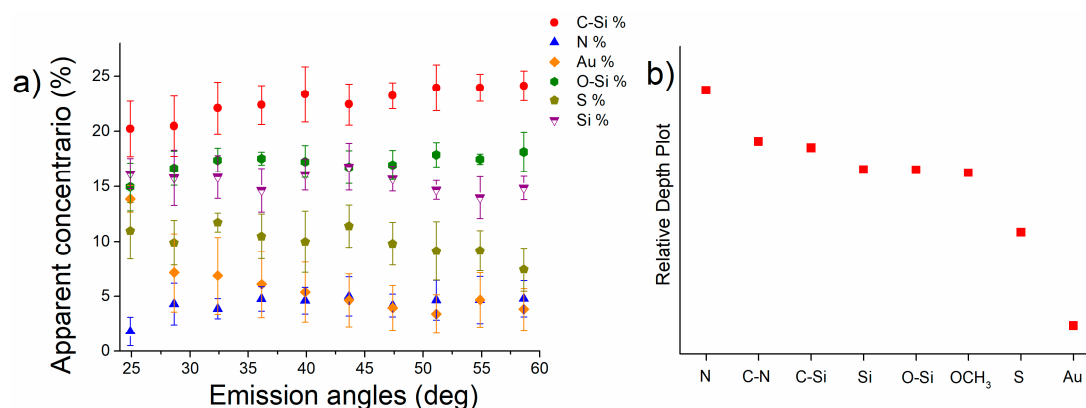


**Figure 9.** Apparent concentration vs emission angles calculated for Au, Si, S, C-Si, O-Si and N of the A-Gold samples (a) and relative depth plot calculated considering the elements: N, Si, O, S and Au of MPTMS and APTES for A-Gold samples (b).

### 3.6. Calculation of the Layer Thickness

The determination of the thickness of the functionalized layer is challenging, and various methodologies employing XPS or ARXPS have been proposed in the literature [16,18,25]. In 1970 Hill et alii introduced a method for measuring film thickness of thin films on a substrate, known as Hill's equation [41]. Hill's equation, denoted as equation 1, can be expressed as follows:

$$I_0 = I_S e^{-\frac{t}{\lambda \cos \theta}} \quad 1)$$

In this equation 't' represents the overlayer thickness, and 'q' is the emission angle. It is assumed that the overlayer is homogeneous and has a uniform thickness, and the attenuation length l of the photoelectrons is considered the same for both the bulk and the overlayer [42].

Since in this work only angles lower than 60 degrees are considered for the thickness estimation by ARXPS data, the elastic scattering effect can be considered negligible and IMFP has been used instead of the attenuation length. Furthermore, this approximation can be made because the thickness of the overlayer is supposed to be lower than the IMFP.

In the case of the system gold/MPTMS/APTES there are no elements in common between the substrate and the functionalization layer, hence eq. 1 cannot be applied. The thickness has been calculated based on ARXPS data considering the attenuation of the intensity  $I_{Au}$  of the Au 4f signal measured at two different emission angles, grazing (58.6 degrees) and near vertical (24.8 degrees). The following equation has been used for the thickness calculation:

$$\ln \left( \frac{I_{Au24^\circ}}{I_{Au58^\circ}} \right) = -\frac{t}{\lambda_{Au}} \left( \frac{1}{\cos(58)} - \frac{1}{\cos(24)} \right) \quad 2)$$

$$t = \frac{\ln\left(\frac{I_{Au24^\circ}}{I_{Au58^\circ}}\right) \cdot \lambda_{Au}}{\cos(24) - \cos(58)} \quad 3)$$

The same formula was applied using instead of the gold Au 4f signal, the intensity of the sulphur S 2p and of the silicon 2p for M-Gold, and for N 1s for A-Gold to calculate the respective thicknesses. The inelastic mean free path (IMFP) of the elements was calculated according to Seah and Dench [32]. The thickness values calculated on three different analysed areas of three independent samples are shown in Table 4.

**Table 4.** Total thickness of the overlayers calculated on M-gold and A-gold based on the attenuation of the elements Au, S, Si and N according to equation 3.

Element	Au	S	Si	N
IMFP l (nm)	2.02	3.16	3.24	3.06
Thickness M-Gold (nm)	1.9 (0.3)	1.4 (0.3)	1.1 (0.2)	-
Thickness A-Gold (nm)	1.8 (0.3)	1.2 (0.4)	0.6 (0.2)	0.3 (0.1)

Regarding M-Gold, the total thickness was calculated using the attenuation of the gold signal and it is found to be 1.9 (0.3) nm; this value includes the thickness of the MPTMS layer, that of the contamination layer  $l_c$ , and the gold substrate. Considering the attenuation of the Si 2p electrons the thickness determined is the sum of the contamination layer  $l_c$  and of O-CH<sub>3</sub> groups and its value is 1.1 (0.2) nm.

The same considerations applied to A-Gold samples, the total thickness is calculated to be 1.8 (0.3) nm, and the layer thickness calculated by considering the attenuation of the N 1s electrons was estimated to be 0.3 (0.1) nm. This might suggest that the thickness of the contamination layer,  $l_c$ , is much lower than on M-Gold samples with the MPTMS layer (see discussion section 4.3.1).

## 4. Discussion

### 4.1. Understanding APTES Functionalization Mechanisms

In literature, the reaction between MPTMS and APTES is reported [4] and, according to the expected stoichiometry, the sulphur to nitrogen ratio should be 1:1. However, the results of the quantitative analysis (Table 3) showed a sulphur to nitrogen ratio equal to 2:1, suggesting a different reaction mechanism. Indeed, in literature numerous examples of SiO<sub>2</sub> substrates functionalized with APTES are reported, proposing different potential behaviour of this molecule during the functionalization process [22,43–45]. Figure 10 (a-d) is a schematic representation of the various possible arrangements that APTES molecules might adopt for obtaining A-Gold samples and in correspondence different reaction pathways can be suggested.

Figure 10a shows the expected result according to [4], but on the basis of the results obtained in this work (Table 3) is not in agreement with this stoichiometry. Also, the reaction schemes shown in Figure 10 b and in Figure 10 c, between three molecules of MPTMS with one of APTES and a ratio of 3:1, can be ruled out on the basis of the experimental results, which lead to a 2 to 1 sulphur to nitrogen ratio. The most probable arrangement of the APTES in A-gold samples is shown in Figure 10d where the ratio of sulphur to nitrogen is 2:1 in agreement with the experimental results (Table 3).

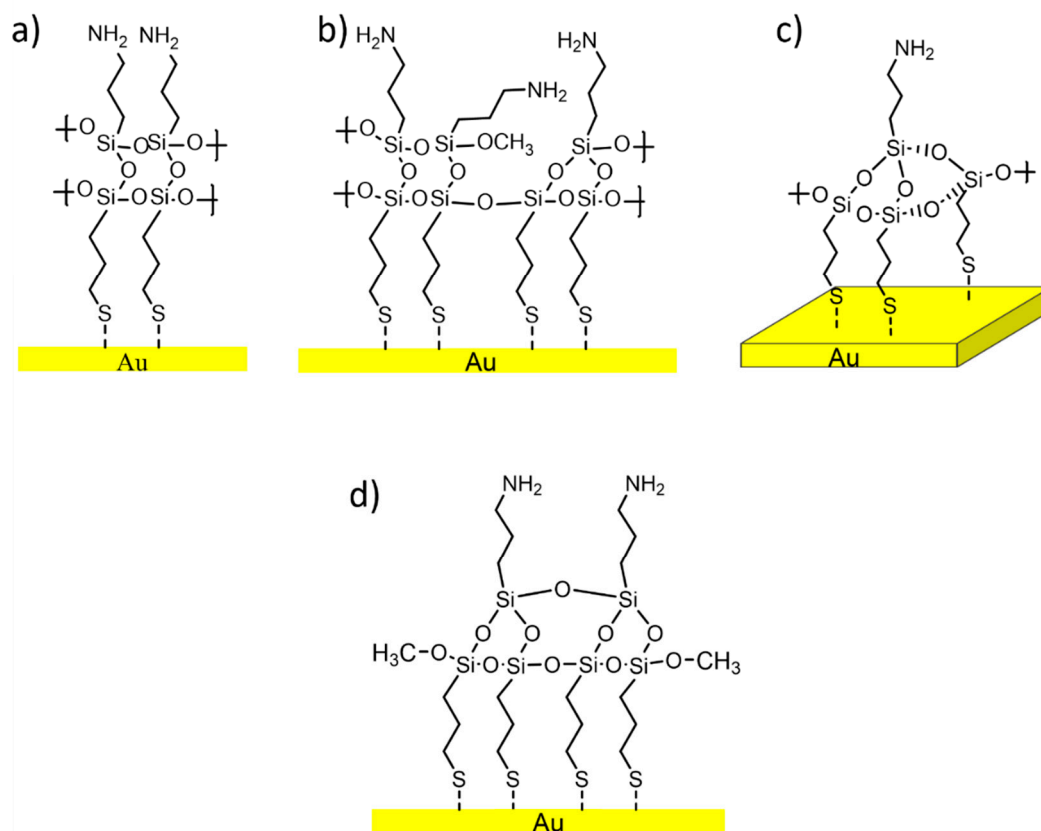


**Figure 10.** Possible arrangement of APTES onto MPTMS functionalized gold surface (M-Gold).

#### 4.2. Models for the Functionalized M-Gold and A-Gold Surfaces

Based on the reaction scheme and the results from ARXPS measurements (relative depth plot in Figure 8b and Figure 9b), the models for the functionalized M-gold (Figure 11a) and A-gold (Figure 11b) are proposed. The model of M-gold consists of three layers: the gold substrate on which the MPTMS is bounded via sulphur and a hydrocarbon contamination layer.

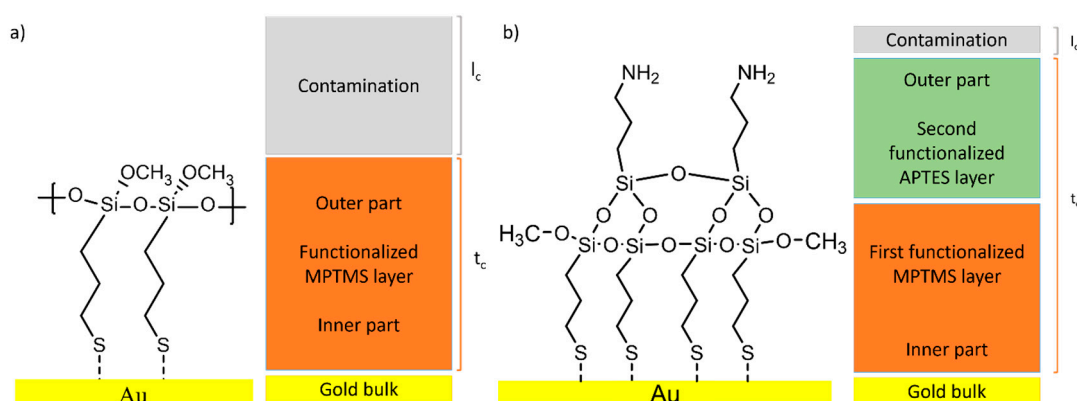


**Figure 11.** Idealized model for MPTMS functionalization (M-gold, a) and MPTMS + APTES functionalization (A-gold, b).

The proposed model for A-gold consists of four layers: the gold substrate, a first functionalized layer of MPTMS and second layer of APTES grafted to the MPTMS surface through the polymerization of the Si-O functional groups, with a thin hydrocarbon contamination layer on top (Figure 11b).

### 4.3. Thickness and Composition of the Functionalized Layers

#### 4.3.1. Layer Thickness

Based on the ARXPS results the total thickness layer calculated on M-Gold samples with equation (3) is  $1.9 \pm 0.3$  nm (Table 4). The total thickness is the result of the sum of the contamination layer ( $l_c$ ), and the functionalization layer of MPTMS ( $t$ ) as depicted in Figure 11. Exploiting equation (3) considering the attenuation of sulphur signal (Table 4), the total thickness results of  $1.4 \pm 0.3$  nm, thus comprises the MPTMS layer and the contamination layer. Using the same equation and considering silicon, a thickness of  $1.1 \pm 0.2$  nm has been calculated. This value consists of  $l_c$  summed to the  $-OCH_3$  groups located at the outer part of the MPTMS layer. Avogadro software calculation estimate the bond length of  $-OCH_3$  groups to be 0.2 nm, thus the  $l_c$  contamination layer thickness can be estimated to be 0.9 nm. As shown in Table 5, the thickness calculated of MPTMS layer  $t$  can be estimated to be equal to 0.5 nm (thickness calculated from the attenuation of the sulphur (1.4 nm) minus the  $l_c$  estimated to be 0.9 nm). The chain length of the MPTMS molecule has been calculated by means of Avogadro software, and the distance between sulphur and silicon has been found to be 0.47 nm. The results are summarized in Table 5 and are in good agreement with the experimental data [46].

**Table 5.** Summary of the thickness of the functionalized layer and the contamination layer on gold and on PVC (accuracy  $\pm 0.2$  nm).

Layer	Freshly cleaved gold	MPTMS on PVC [46]	MPTMS on gold	MPTMS + APTES on gold
Contamination $l_c$	0.4 nm	1.1 nm	0.9 nm	0.3 nm
Layer thickness $t$	-	0.5 nm	0.5 nm	1.0 nm
Avogadro calculation	-	0.7 nm	0.47 nm	1.0 nm

Based on the results found on M-gold samples, the same considerations have been made for A-Gold samples (Figure 11). Calculating the attenuation of sulphur signal with equation (3) a layer thickness of  $1.2 \pm 0.4$  nm was estimated (Table 4), including the MPTMS+APTES functionalization layer and the contamination layer. Based on the attenuation of nitrogen photoelectrons (emitted from the outer part of the functionalization layer), a layer thickness of  $0.3 \pm 0.1$  nm was calculated. Thus, the contamination layer thickness  $l_c$  can be estimated for A-Gold to be about of 0.3 nm. Subtracting the contamination layer  $l_c$  from the total thickness calculated with sulphur of 1.2 nm (Table 4), an overlayer thickness  $t$  of about 0.9 - 1 nm can be estimated (Table 5). The Avogadro simulation estimates a distance between sulphur of the MPTMS layer and the nitrogen of the APTES layer of 1 nm. The results are summarized in Table 5 and are in good agreement with the experimental data. In both cases of functionalized gold surface and of MPTMS on PVC [46] the experimental results agree with the Avogadro simulations.

We note here a much lower thickness of the contamination layer  $l_c$  on A-gold (Table 5). This result might be attributed to the nitrogen atoms at the outermost surface of the functionalized A-gold (Figure 11b) that can partially react with the atmospheric  $CO_2$ , resulting in the formation of  $NHCOO$  carbamate as revealed by a small signal in the nitrogen N 1s spectrum (Figure 7c, Table 3) and in C 1s signal (Figure 7b, Table 3). The polar group of carbamate hinders the formation of a thick contamination layer, as has been found for APTES monolayer on silicon substrate [24], where the thickness of the contamination layer is reported to range between 0.1 and 0.5 nm.

The thickness calculated with Au, S and Si for A-gold samples are lower than the one calculated on M-gold samples, these results can be explained considering the Avogadro calculation. In fact, the distance between silicon and nitrogen after the formation of the second layer with APTES measured by Avogadro is 0.44 nm, the attenuation of the N 1s electrons was estimated to be 0.3 nm thus suggesting that assuming the formation of a second layer with no tilt angle the total thickness of the APTES layer (APTES +  $l_c$ ) is around 0.74 nm, while on M-Gold was found a contamination layer of

0.9 nm. Moreover, the distance between sulphur atoms and silicon atoms measured on Avogadro after the addition of the APTES layer slightly decreases and it is estimated by the software to be 0.41 nm and not 0.47 nm as estimated in the simulation of the MPTMS samples on gold.

#### 4.3.2. Composition of the Functionalized Layers

Based on the models proposed for the functionalized surfaces M-gold and A-gold (Figure 11) the expected composition of the functionalized MPTMS and MPTMS+APTES surfaces can be calculated and compared with the data determined by XPS (Table 5). A very good agreement between the expected and the experimental values is found, thus substantiating the models proposed in Figure 11.

**Table 5.** Experimental (mean value and standard deviation calculated over results obtained on three different areas of three independent samples) and calculated composition of the functionalized layer M-gold and A-gold.

Functional group	M-gold (at%)		A-gold (at %)	
	Experimental	Calculated	Experimental	Calculated
C-Si, C-C	27 (2)	24	27 (1)	30
C-S	13 (1)	12	13 (1)	15
C Methoxide	4 (1)	12	4 (1)	-
O-C=O carbamate	-	-	1.3 (0.2)	-
Si-O-Si	29 (2)	29	23 (2)	23
S	13 (2)	12	10 (2)	10
Si	13 (2)	12	15 (1)	15
-NH <sub>2</sub>	-	-	3 (1)	5
NHCOO	-	-	1.3 (0.4)	-
-NH <sub>3</sub> <sup>+</sup>	-	-	0.5 (0.1)	-

In M-gold sample the binding energy of the S 2p<sub>3/2</sub> component was found to be 163.7 (0.1) eV (Table 2). In the literature, Au-S bond for long chain thiolate is reported to range between 162-163 eV [47]; the discrepancy between the literature and the experimental results may be related to the functionalization conditions adopted in this work and especially to the short immersion time of the gold substrate in the MPTMS solutions to mimic the conditions adopted in the case of food-grade PVC.

In the literature the S 2p<sub>3/2</sub> component at binding energy higher than the one ascribed to alkyl thiolate has been assigned to unbound thiolates [47] and/or to disulphides [48]. Some papers defined those compounds as physisorbed molecules [48,49]. According to these authors, the high binding energy component should not be present in the S 2p spectra of "good quality SAM" and the physisorbed molecules should be located at the SAM-ambient interface [49,50]. In this work, the presence of the component at 162 eV was not detected, but angle-resolved XPS data (Figures 8 and 9) clearly indicate that the in-depth distribution of the functional groups follows the expected reaction schemes shown in Figures 1 and 2. Recently it was demonstrated that, in SAM obtained by solution deposition, the gold-sulfur bond has not a chemisorbed character and that hydrogen in -SH is retained [51]. On the other hand the presence of the electronegative O-Si-O functional group of MPTMS can also play a role in the observed chemical shift; in fact, similar binding energy (163.8 eV) have been reported for gold nanoparticles modified with MPTMS [52].

Tri-dimensional networking should also be taking into account because of the presence of water.

Changes in the molecular structure (Fig. 11) might induce also changes in the binding energy of the different elements. After the grafting of APTES on M-gold surface, the binding energy of the C-Si, CH<sub>2</sub> as well as the Si 2p and S 2p signal slightly increased by 0.4 eV (Table 3, A-gold) compared to M-gold samples (Table 2). This chemical shift can be explained considering the cross-linking between the Si-O groups of MPTMS and APTES; in fact similar chemical shift for the silicon have been observed in the case of APTES monolayer on silicon oxide surface [53]. As mentioned in section 4.3.1

Avogadro simulation suggest that after the formation of the APTES layer, the distance between sulphur atoms and the Si-O-Si groups decreases from 0.47 nm to 0.41 nm, thus can also justify the chemical shift of the S 2p signal, in fact its BE can be affected by the proximity of the oxygen atoms of the Si-O-Si groups.

#### 4.4. Parameter Identification for Developing a Transferable Analytical Strategy in Polymeric Systems

XPS and ARXPS characterization of functionalized surface layers on realistic substrates such as polymers or carbon-based materials modified with MPTMS and APTES is challenging due to the simultaneous presence of signals both from the substrate and the functionalized layers. The use of a freshly cleaved gold as carbon-free model substrate with an ideally flat surface is pivotal for the determination of the curve-fitting parameters, especially for the C 1s spectrum. Avoiding the interference of signals from carbon atoms present in the substrate (such as e.g. PVC), the signals in the C1s spectrum can be assigned to the MPTMS / APTES functionalized layer only.

Processing XPS and ARXPS high-resolution spectra starts with background subtraction. In this work, U 3 Tougaard background was selected to better simulate the required conditions for the polymer surface characterization [29]. Parameters for the subsequent curve fitting procedure, especially signal shape (G/L ratio), FWHM and area ratios, were determined for all signals in the C 1s, O 1s, Si 2p, S 2p and N 1s high-resolution spectra. This allowed the identification of the components that can be assigned to the functionalization layer. The mechanism when grafting MPTMS with APTES was found to be a 2 MPTMS : 1 APTES reaction as confirmed by the quantitative analysis. This analytical strategy has been successfully employed in characterizing an MPTMS monolayer on a food-grade PVC surface as described in a recent work [46]; more generally, it can be a powerful tool for characterizing the functionalized surface of more complex systems.

## 5. Conclusions

Based on these findings the following conclusions can be drawn:

1. The detailed analysis of the XPS high-resolution spectra allowed understanding the overlayer formation of MPTMS first, and MPTMS+APTES onto freshly cleaved gold surfaces. The quantitative analysis suggests the functionalization of the gold surface with MPTMS was successful and homogeneous. The at% of the CH<sub>3</sub>O was found to be 4% instead of 12% expected from the stoichiometry suggesting a three-dimensional cross-linking of the Si-O-Si bond. After the grafting of APTES onto the M-gold surface, quantitative analysis was in good agreement with the stoichiometry considering a ratio MPTMS:APTES of 2:1.
2. Angle-resolved XPS allowed understanding the in-depth distribution of the overlayer functional groups after the two functionalization steps. Based on these results a model of the functionalized surface was proposed and consists of a first layer of MPTMS (after the first step) with the Si-O groups facing the outer part of the surface. Following the grafting of the APTES onto the M-gold surface ARXPS results indicate that APTES react with MPTMS through Si-O groups facing the amino groups in the outer part of the functionalization layer. Furthermore, through the ARXPS results have been possible to a 1 nm layer of MPTMS+APTES.
3. The analytical strategy presented in this work based on XPS and ARXPS by using gold as a carbon-free substrate represents a useful tool for a proper curve fitting of C 1s signal and layer thickness estimation to be adopted for similar systems with carbon-based substrate such as polymer.

**Supplementary Materials:** The following supporting information can be downloaded at the website of this paper posted on Preprints.org.

**Acknowledgements:** The authors are grateful to: MIUR- Fondo per lo Sviluppo e la Coesione FSC-Piano Stralcio 2015/2017 for the Ph.D. grant assigned to Mr. Giulio Casula (Consortium UniCa and UniSS); – Project number CUP J89J20000930001 (2021): “Functionalization of Food Packaging with active antimicrobial agent” and to the University of Cagliari (UniCA) and Fondazione di Sardegna (FdS) for the financial support UNICA-FdS

(Fondazione di Sardegna) 2019 – Project number CUP J89J20000930001. Dottor Cristiana Passiu for the preparation of the gold surfaces used in this work

## References

1. Vericat, C.; Vela, M.E.; Benitez, G.; Carro, P.; Salvarezza, R.C. Self-Assembled Monolayers of Thiols and Dithiols on Gold: New Challenges for a Well-Known System. *Chem. Soc. Rev.* **2010**, *39*, 1805–1834, doi:10.1039/B907301A.
2. Spencer, N.D. *Tailoring Surfaces: Modifying Surface Composition and Structure for Applications in Tribology, Biology and Catalysis*; Co-Published with Indian Institute of Science (IISc), Bangalore, India, 2011; ISBN 978-981-4289-42-9.
3. Xia, Y.; Zhao, X.-M.; Whitesides, G.M. Pattern Transfer: Self-Assembled Monolayers as Ultrathin Resists. *Microelectronic Engineering* **1996**, *32*, 255–268, doi:10.1016/0167-9317(95)00174-3.
4. Villanueva, M.E.; González, J.A.; Rodríguez-Castellón, E.; Teves, S.; Copello, G.J. Antimicrobial Surface Functionalization of PVC by a Guanidine Based Antimicrobial Polymer. *Materials Science and Engineering: C* **2016**, *67*, 214–220, doi:10.1016/j.msec.2016.05.052.
5. Love, J.C.; Estroff, L.A.; Kriebel, J.K.; Nuzzo, R.G.; Whitesides, G.M. Self-Assembled Monolayers of Thiolates on Metals as a Form of Nanotechnology. *Chem. Rev.* **2005**, *105*, 1103–1170, doi:10.1021/cr0300789.
6. Gothe, P.K.; Gaur, D.; Achanta, V.G. MPTMS Self-Assembled Monolayer Deposition for Ultra-Thin Gold Films for Plasmonics. *J. Phys. Commun.* **2018**, *2*, 035005, doi:10.1088/2399-6528/aaaedd.
7. Piwoński, I.; Grobelny, J.; Cichowski, M.; Celichowski, G.; Rogowski, J. Investigation of 3-Mercaptopropyltrimethoxysilane Self-Assembled Monolayers on Au(111) Surface. *Applied Surface Science* **2005**, *242*, 147–153, doi:10.1016/j.apsusc.2004.08.009.
8. Kumar, S.; Soni, S.; Danowski, W.; van Beek, C.L.F.; Feringa, B.L.; Rudolf, P.; Chiechi, R.C. Correlating the Influence of Disulfides in Monolayers across Photoelectron Spectroscopy Wettability and Tunneling Charge-Transport. *J. Am. Chem. Soc.* **2020**, *142*, 15075–15083, doi:10.1021/jacs.0c06508.
9. Lees, W.J.; Whitesides, G.M. Equilibrium Constants for Thiol-Disulfide Interchange Reactions: A Coherent, Corrected Set. *J. Org. Chem.* **1993**, *58*, 642–647, doi:10.1021/jo00055a016.
10. Azzam, W.; Bashir, A.; Biedermann, P.U.; Rohwerder, M. Formation of Highly Ordered and Orientated Gold Islands: Effect of Immersion Time on the Molecular Adlayer Structure of Pentafluorobenzenethiols (PFBT) SAMs on Au(111). *Langmuir* **2012**, *28*, 10192–10208, doi:10.1021/la301601c.
11. Cortés, E.; Rubert, A.A.; Benitez, G.; Carro, P.; Vela, M.E.; Salvarezza, R.C. Enhanced Stability of Thiolate Self-Assembled Monolayers (SAMs) on Nanostructured Gold Substrates Available online: <https://pubs.acs.org/doi/full/10.1021/la804251a> (accessed on 12 February 2024).
12. Yang, Y.; Qing, Y.; Hao, X.; Fang, C.; Ouyang, P.; Li, H.; Wang, Z.; Liao, Y.; Fang, H.; Du, J. APTES-Modified Remote Self-Assembled DNA-Based Electrochemical Biosensor for Human Papillomavirus DNA Detection. *Biosensors* **2022**, *12*, 449, doi:10.3390/bios12070449.
13. Villanueva, M.E.; Salinas, A.; González, J.A.; Teves, S.; Copello, G.J. Dual Antibacterial Effect of Immobilized Quaternary Ammonium and Aliphatic Groups on PVC. *New J. Chem.* **2015**, *39*, 9200–9206, doi:10.1039/C5NJ01766A.
14. Krishna, D.N.G.; Philip, J. Review on Surface-Characterization Applications of X-Ray Photoelectron Spectroscopy (XPS): Recent Developments and Challenges. *Applied Surface Science Advances* **2022**, *12*, 100332, doi:10.1016/j.apsadv.2022.100332.
15. Watts, J.F.; Wolstenholme, J. *An Introduction to Surface Analysis by XPS and AES*; John Wiley & Sons, 2019; ISBN 978-1-119-41758-3.
16. Briggs, D. *Surface Analysis of Polymers by XPS and Static SIMS*; Cambridge Solid State Science Series; Cambridge University Press: Cambridge, 1998; ISBN 978-0-521-35222-2.
17. Afanas'ev, V.P.; Selyakov, D.N.; Ridzel, O.Y.; Semenov-Shefov, M.A.; Strukov, A.N. Investigation of Monolayer and Submonolayer Films Using X-Ray Photoelectron Spectroscopy. *J. Phys.: Conf. Ser.* **2020**, *1713*, 012002, doi:10.1088/1742-6596/1713/1/012002.
18. Parry, K.L.; Shard, A.G.; Short, R.D.; White, R.G.; Whittle, J.D.; Wright, A. ARXPS Characterisation of Plasma Polymerised Surface Chemical Gradients. *Surface and Interface Analysis* **2006**, *38*, 1497–1504, doi:10.1002/sia.2400.

19. Spori, D.M.; Venkataraman, N.V.; Tosatti, S.G.P.; Durmaz, F.; Spencer, N.D.; Zürcher, S. Influence of Alkyl Chain Length on Phosphate Self-Assembled Monolayers. *Langmuir* **2007**, *23*, 8053–8060, doi:10.1021/la700474v.
20. Chen, H.; Heng, C.K.; Puiu, P.D.; Zhou, X.D.; Lee, A.C.; Lim, T.M.; Tan, S.N. Detection of *Saccharomyces Cerevisiae* Immobilized on Self-Assembled Monolayer (SAM) of Alkanethiolate Using Electrochemical Impedance Spectroscopy. *Analytica Chimica Acta* **2005**, *554*, 52–59, doi:10.1016/j.aca.2005.08.086.
21. Gates, B.D.; Xu, Q.; Stewart, M.; Ryan, D.; Willson, C.G.; Whitesides, G.M. New Approaches to Nanofabrication: Molding, Printing, and Other Techniques. *Chem. Rev.* **2005**, *105*, 1171–1196, doi:10.1021/cr030076o.
22. Piwoński, I.; Grobelny, J.; Cichomski, M.; Celichowski, G.; Rogowski, J. Investigation of 3-Mercaptopropyltrimethoxysilane Self-Assembled Monolayers on Au(111) Surface. *Applied Surface Science* **2005**, *242*, 147–153, doi:10.1016/j.apsusc.2004.08.009.
23. Penna, A.; Careri, M.; Spencer, N.D.; Rossi, A. Effects of Tailored Surface Chemistry on Desorption Electrospray Ionization Mass Spectrometry: A Surface-Analytical Study by XPS and AFM. *J. Am. Soc. Mass Spectrom.* **2015**, *26*, 1311–1319, doi:10.1007/s13361-015-1135-9.
24. Graf, N.; Yegen, E.; Gross, T.; Lippitz, A.; Weigel, W.; Krakert, S.; Terfort, A.; Unger, W.E.S. XPS and NEXAFS Studies of Aliphatic and Aromatic Amine Species on Functionalized Surfaces. *Surface Science* **2009**, *603*, 2849–2860, doi:10.1016/j.susc.2009.07.029.
25. Walton, J.; Alexander, M.R.; Fairley, N.; Roach, P.; Shard, A.G. Film Thickness Measurement and Contamination Layer Correction for Quantitative XPS. *Surface and Interface Analysis* **2016**, *48*, 164–172, doi:10.1002/sia.5934.
26. Naik, V.V.; Crobu, M.; Venkataraman, N.V.; Spencer, N.D. Multiple Transmission-Reflection IR Spectroscopy Shows That Surface Hydroxyls Play Only a Minor Role in Alkylsilane Monolayer Formation on Silica. *J. Phys. Chem. Lett.* **2013**, *4*, 2745–2751, doi:10.1021/jz401440d.
27. Passiu, C.; Rossi, A.; Bernard, L.; Paul, D.; Hammond, J.; Unger, W.E.S.; Venkataraman, N.V.; Spencer, N.D. Fabrication and Microscopic and Spectroscopic Characterization of Planar, Bimetallic, Micro- and Nanopatterned Surfaces. *Langmuir* **2017**, *33*, 5657–5665, doi:10.1021/acs.langmuir.7b00942.
28. Passiu, C.; Rossi, A.; Weinert, M.; Tysoe, W.; Spencer, N.D. Probing the Outermost Layer of Thin Gold Films by XPS and Density Functional Theory. *Applied Surface Science* **2020**, *507*, 145084, doi:10.1016/j.apsusc.2019.145084.
29. Tougaard, S. Practical Guide to the Use of Backgrounds in Quantitative XPS. *Journal of Vacuum Science & Technology A* **2021**, *39*, 011201, doi:10.1116/6.0000661.
30. Scofield, J.H. Hartree-Slater Subshell Photoionization Cross-Sections at 1254 and 1487 eV. *Journal of Electron Spectroscopy and Related Phenomena* **1976**, *8*, 129–137, doi:10.1016/0368-2048(76)80015-1.
31. Zommer, L. Determination of the Spectrometer Transmission Function for XPS Quantitative Analysis. *Vacuum* **1995**, *46*, 617–620, doi:10.1016/0042-207X(94)00143-X.
32. Seah, M.P.; Dench, W.A. Quantitative Electron Spectroscopy of Surfaces: A Standard Data Base for Electron Inelastic Mean Free Paths in Solids. *Surface and Interface Analysis* **1979**, *1*, 2–11, doi:10.1002/sia.740010103.
33. Gunter, P.L.J.; Gijzeman, O.L.J.; Niemantsverdriet, J.W. Surface Roughness Effects in Quantitative XPS: Magic Angle for Determining Overlay Thickness. *Applied Surface Science* **1997**, *115*, 342–346, doi:10.1016/S0169-4332(97)00007-X.
34. Engelhard, M.H.; Baer, D.R.; Herrera-Gomez, A.; Sherwood, P.M.A. Introductory Guide to Backgrounds in XPS Spectra and Their Impact on Determining Peak Intensities. *Journal of Vacuum Science & Technology A: Vacuum, Surfaces, and Films* **2020**, *38*, 063203, doi:10.1116/6.0000359.
35. Fairley, N.; Fernandez, V.; Richard-Plouet, M.; Guillot-Deudon, C.; Walton, J.; Smith, E.; Flahaut, D.; Greiner, M.; Biesinger, M.; Tougaard, S.; et al. Systematic and Collaborative Approach to Problem Solving Using X-Ray Photoelectron Spectroscopy. *Applied Surface Science Advances* **2021**, *5*, 100112, doi:10.1016/j.apsadv.2021.100112.
36. Fracassi, A.; Ray, A.; Nakatsuka, N.; Passiu, C.; Tanriver, M.; Schauenburg, D.; Scherrer, S.; Ouald Chaib, A.; Mandal, J.; Ramakrishna, S.N.; et al. KAT Ligation for Rapid and Facile Covalent Attachment of Biomolecules to Surfaces. *ACS Appl. Mater. Interfaces* **2021**, *13*, 29113–29121, doi:10.1021/acsami.1c05652.
37. Li, Y.-S.; Lu, W.; Wang, Y.; Tran, T. Studies of (3-Mercaptopropyl)Trimethoxysilane and Bis(Trimethoxysilyl)Ethane Sol–Gel Coating on Copper and Aluminum. *Spectrochimica Acta Part A: Molecular and Biomolecular Spectroscopy* **2009**, *73*, 922–928, doi:10.1016/j.saa.2009.04.016.

38. Silva, F.S. da; Melo, H.G. de; Benedetti, A.V.; Suegama, P.H. Influence of Ce(IV) Ions Amount on the Electrochemical Behavior of Organic-Inorganic Hybrid Coatings in 0.1 Mol L<sup>-1</sup> NaCl Solution. *Eclética Química* **2019**, *44*, 27–56.
39. Ederer, J.; Janoš, P.; Ecorchard, P.; Tolasz, J.; Štengl, V.; Beneš, H.; Perchacz, M.; Pop-Georgievski, O. Determination of Amino Groups on Functionalized Graphene Oxide for Polyurethane Nanomaterials: XPS Quantitation vs. Functional Speciation. *RSC Adv.* **2017**, *7*, 12464–12473, doi:10.1039/C6RA28745J.
40. Stegmeier, S.; Fleischer, M.; Tawil, A.; Hauptmann, P.; Egly, K.; Rose, K. Mechanism of the Interaction of CO<sub>2</sub> and Humidity with Primary Amino Group Systems for Room Temperature CO<sub>2</sub> Sensors. *Procedia Chemistry* **2009**, *1*, 236–239, doi:10.1016/j.proche.2009.07.059.
41. Hill, J.M.; Royce, D.G.; Fadley, C.S.; Wagner, L.F.; Grunthaner, F.J. Properties of Oxidized Silicon as Determined by Angular-Dependent X-Ray Photoelectron Spectroscopy. *Chemical Physics Letters* **1976**, *44*, 225–231, doi:10.1016/0009-2614(76)80496-4.
42. Brundle, C.R.; Conti, G.; Mack, P. XPS and Angle Resolved XPS, in the Semiconductor Industry: Characterization and Metrology Control of Ultra-Thin Films. *Journal of Electron Spectroscopy and Related Phenomena* **2010**, *178–179*, 433–448, doi:10.1016/j.elspec.2010.03.008.
43. XPS and NEXAFS Studies of Aliphatic and Aromatic Amine Species on Functionalized Surfaces | Elsevier Enhanced Reader Available online: <https://reader.elsevier.com/reader/sd/pii/S0039602809005068?token=F8A8BC084615658A974BD13927A0D9267C67AEF99FD405F53A180FB8D52092A0CE7105DCF3DF3BC1C5B9A0FB7034191E&originRegion=eu-west-1&originCreation=20220922072105> (accessed on 22 September 2022).
44. Sui, W.; Zhao, W.; Zhang, X.; Peng, S.; Zeng, Z.; Xue, Q. Comparative Anti-Corrosion Properties of Alkylthiols SAMs and Mercapto Functional Silica Sol–Gel Coatings on Copper Surface in Sodium Chloride Solution. *J Sol-Gel Sci Technol* **2016**, *80*, 567–578, doi:10.1007/s10971-016-4108-y.
45. Sypabekova, M.; Hagemann, A.; Rho, D.; Kim, S. Review: 3-Aminopropyltriethoxysilane (APTES) Deposition Methods on Oxide Surfaces in Solution and Vapor Phases for Biosensing Applications. *Biosensors* **2023**, *13*, 36, doi:10.3390/bios13010036.
46. Casula, G.; Fantauzzi, M.; Elsener, B.; Rossi, A. Surface Modification of Food-Grade PVC Monitored by Angle-Resolved XPS. *Vacuum* **2024**, 113010, doi:10.1016/j.vacuum.2024.113010(in press).
47. Castner, D.G.; Hinds, K.; Grainger, D.W. X-Ray Photoelectron Spectroscopy Sulfur 2p Study of Organic Thiol and Bisulfide Binding Interactions with Gold Surfaces. *Langmuir* **1996**, *12*, 5083–5086, doi:10.1021/la960465w.
48. Cristina, L.J.; Ruano, G.; Salvarezza, R.; Ferrón, J. Thermal Stability of Self-Assembled Monolayers of n-Hexanethiol on Au(111)-(1 × 1) and Au(001)-(1 × 1). *J. Phys. Chem. C* **2017**, *121*, 27894–27904, doi:10.1021/acs.jpcc.7b05883.
49. Watcharinyanon, S.; Nilsson, D.; Moons, E.; Shaporenko, A.; Zharnikov, M.; Albinsson, B.; Mårtensson, J.; Johansson, L.S.O. A Spectroscopic Study of Self-Assembled Monolayer of Porphyrin-Functionalized Oligo(Phenyleneethynylene)s on Gold: The Influence of the Anchor Moiety. *Phys. Chem. Chem. Phys.* **2008**, *10*, 5264–5275, doi:10.1039/B802914H.
50. Jia, J.; Kara, A.; Pasquali, L.; Bendounan, A.; Sirotti, F.; Esaulov, V.A. On Sulfur Core Level Binding Energies in Thiol Self-Assembly and Alternative Adsorption Sites: An Experimental and Theoretical Study. *J Chem Phys* **2015**, *143*, 104702, doi:10.1063/1.4929350.
51. Inkpen, M.S.; Liu, Z.-F.; Li, H.; Campos, L.M.; Neaton, J.B.; Venkataraman, L. Non-Chemisorbed Gold–Sulfur Binding Prevails in Self-Assembled Monolayers. *Nat. Chem.* **2019**, *11*, 351–358, doi:10.1038/s41557-019-0216-y.
52. Wu, P.; Peng, B.; Yan, Z.; Zhao, X. Gold Nanoparticles Supported on Mesoporous Silica: Origin of High Activity and Role of Au NPs in Selective Oxidation of Cyclohexane. *Scientific Reports* **2016**, *6*, 18817, doi:10.1038/srep18817.
53. Dietrich, P.M.; Glamsch, S.; Ehlert, C.; Lippitz, A.; Kulak, N.; Unger, W.E.S. Synchrotron-Radiation XPS Analysis of Ultra-Thin Silane Films: Specifying the Organic Silicon. *Applied Surface Science* **2016**, *363*, 406–411, doi:10.1016/j.apsusc.2015.12.052.

**Disclaimer/Publisher's Note:** The statements, opinions and data contained in all publications are solely those of the individual author(s) and contributor(s) and not of MDPI and/or the editor(s). MDPI and/or the editor(s)

disclaim responsibility for any injury to people or property resulting from any ideas, methods, instructions or products referred to in the content.